Effects of water and ice clouds on cloud microphysical budget: An equilibrium modeling study*

Gao Shou-Ting(高守亭)[a], Li Xiao-Fan(李小凡)[b], and Zhou Yu-Shu(周玉淑)[a]†

[a] *Laboratory of Cloud-Precipitation Physics and Severe Storms (LACS), Institute of Atmospheric Physics, Chinese Academy of Sciences, Beijing* 100029, *China*

[b] *Department of Earth Sciences, Zhejiang University, Hangzhou* 310027, *China*

(Received 25 March 2013; revised manuscript received 19 April 2013; published online 10 December 2013)

The effects of water and ice clouds on the cloud microphysical budget associated with rainfall are investigated through the analysis of grid-scale data from a series of two-dimensional cloud-resolving model equilibrium sensitivity simulations. The model is imposed without large-scale vertical velocity. In the control experiment, the contribution from rainfall (cM) associated with net evaporation and hydrometeor loss/convergence is about 29% of that from the rainfall (Cm) associated with net condensation and hydrometeor gain/divergence and about 39% of that from the rainfall (CM) associated with net condensation and hydrometeor loss/convergence. The exclusion of ice clouds enhances rainfall contribution of CM, whereas it reduces rainfall contributions of Cm and cM. The removal of radiative effects of water clouds increases rainfall contribution of CM, barely changes rainfall contribution of Cm and reduces the rainfall contribution of cM in the presence of the radiative effects of ice clouds. Elimination of the radiative effects of water clouds reduces the rainfall contributions of CM and Cm, whereas it increases the rainfall contribution of cM in the absence of the radiative effects of ice clouds.

Keywords: effects of water and ice clouds, cloud budget, net condensation, hydrometeor change/convergence

PACS: 42.68.Ge, 92.60.N–, 92.60.jf, 92.60.Wc **DOI:** 10.1088/1674-1056/23/2/024204

1. Introduction

Precipitation systems have strong upward motions throughout the troposphere, which produce both water and ice clouds (convective clouds) during the development period.[1] Water clouds gradually dissipate and ice clouds (stratiform clouds) play a major role in producing the precipitation during the decay phase. Thus, the precipitation is generally partitioned into convective and stratiform components. Convective rainfall is associated with a higher rain rate, stronger upward motions and horizontal reflectivity gradients than stratiform rainfall; convective and stratiform rainfalls are primarily generated by the accretion of cloud water by raindrops via collisions in strong updraft cores and the vapor deposition on ice particles, respectively.[2] The separation between convective and stratiform rainfall is based on the amplitude and spatial variations of radar reflectivity or surface rainfall data.[3–7] Cui and Li[8] applied the surface rainfall budget proposed by Gao *et al.*[9] to the analysis of a two-dimensional (2D) cloud-resolving model simulation during a select period of the tropical ocean global atmosphere coupled ocean atmosphere response experiment (TOGA COARE); they found that convective rainfall has water vapor convergence whereas stratiform rainfall has local atmospheric drying and the transport of hydrometeor concentration from convective regions to raining stratiform regions. Shen *et al.*[10] further used the surface rainfall budget to separate rainfall in the same COARE experiment and revealed that about 68% of convective rainfall has water vapor convergence. About 57% of stratiform rainfall has local atmospheric drying and 77% of stratiform rainfall is associated with the transport of hydrometeor concentration from convective regions to raining stratiform regions, but only 44% of stratiform rainfall has both local atmospheric drying and the transport of hydrometeor concentration from convective regions to raining stratiform regions. Li and Gao[11] used cloud budget to partition rainfall in the same COARE simulation and showed that the convective rainfall is primarily associated with net condensation, whereas the stratiform rainfall is primarily related to net evaporation and the transport of hydrometeor concentration from convective regions to raining stratiform regions.

As ingredients of precipitation producers, water and ice clouds affect rainfall through cloud microphysical processes and hydrometeor advections, which are major terms in a cloud microphysical budget. Thus, effects of water and ice clouds on cloud microphysical budget associated with equilibrium precipitation are investigated through the analysis of rainfall simulation data in this study. Since large-scale vertical velocity imposed in a cloud-resolving model includes effects from water and ice clouds, the cloud-resolving model simulation data from Gao *et al.*,[12] Ping *et al.*[13] and Gao[14] from equilibrium simulations imposed without large-scale vertical velocity are analyzed to identify the effects of water and ice clouds on

*Project supported by the National Key Basic Research and Development Project of China (Grant No. 2012CB417201), the National Natural Sciences Foundation of China (Grant Nos. 40930950 41075043, 41275065, and 41075044), and the 985 Program of Zhejiang University (Grant No. 188020+193432602/215).

†Corresponding author. E-mail: zys@mail.iap.ac.cn

© 2014 Chinese Physical Society and IOP Publishing Ltd

precipitation.

The rest of this paper is organized as follows. The model and experiment are briefly described in Section 2. The results are presented in Section 3. Comparison between the analyses using rainfall partitioning schemes of Sui *et al.*,[7] Shen *et al.*[10] and Li and Gao[11] is discussed in Section 4. A summary is given in Section 4.

2. Model and experiment

The cloud-resolving model simulation data from Gao *et al.*,[12] Ping *et al.*,[13] and Gao[14] are analyzed in this study. The model setup and general experiment information are summarized in Table 1; detailed model physics can be found in Ref. [15] by Gao and Li and Ref. [11] by Li and Gao. The control experiment is SST29, which is imposed by time-invariant SST of 29 °C. Other sensitivity experiments are summarized in Table 2. The comparison between SST29NIR and SST29 shows the radiative effects of ice clouds on a cloud budget. The comparisons between SST29NWR and SST29 and between SST29NCR and SST29NIR reveal the radiative effects of water clouds on a cloud budget, respectively, in the presence and absence of the radiative effects of ice clouds. The comparison between SST29NIM and SST29 reveals the effects of ice microphysics on a cloud budget.

The calculations of quasi-equilibrium data from the last 10 days of model integration (day 31–day 40) in Table 3 reveal that the exclusion of the radiative effects of ice clouds increases the model domain mean rain rate from SST29 to SST29NIR through the enhanced mean infrared radiative cooling below 8 km,[16] whereas the removal of the microphysical effect of ice clouds reduces the mean rain rate from SST29NIR to SST29NIM through the reduction in the mean net condensation.[13] The exclusion of the radiative effects of water clouds increases the mean rain rate from SST29 to SST29NWR through the increase in the mean infrared radiative cooling and the mean hydrometeor change from gain in SST29 to loss in SST29NWR, in the presence of the radiative effects of ice clouds, which increases the mean rain rate from SST29NIR to SST29NCR through the hydrometeor change from gain in SST29NIR to loss in SST29NCR in the absence of the radiative effects of ice clouds.[16] The hourly grid-scale data from the equilibrium model simulations in the last 20 days are analyzed in the following discussion.

Following Li *et al.*,[17] a cloud budget can be written as

$$P_{\mathrm{S}} = Q_{\mathrm{NC}} + Q_{\mathrm{CM}}, \tag{1}$$

where

$$\begin{aligned} Q_{\mathrm{NC}} &= ([P_{\mathrm{CND}}] + [P_{\mathrm{DEP}}] + [P_{\mathrm{SDEP}}] + [P_{\mathrm{GDEP}}]) \\ &\quad - ([P_{\mathrm{REVP}}] + [P_{\mathrm{MLTG}}] + [P_{\mathrm{MLTS}}]), \end{aligned} \tag{1a}$$

$$Q_{\mathrm{CM}} = -\frac{\partial [q_5]}{\partial t} - \left[\frac{\partial}{\partial x}(uq_5)\right]. \tag{1b}$$

Table 1. A summary for model setups and basic experiment information.

Model history	The model was originally developed by Soong and Ogura,[18] Soong and Tao,[19] Tao and Simpson[20], and modified by Li *et al.*[1,21] and Sui *et al.*[7,22]
Prognostic equations	Potential temperature, specific humidity, five hydrometeor species, perturbation zonal wind and vertical velocity
Cloud microphysical schemes	Lin *et al.*,[23] Rutledge and Hobbs,[24,25] Tao *et al.*,[26] and Krueger *et al.*[27]
Radiation schemes	Chou *et al.*,[28] Chou *et al.*,[29] Chou and Suarez[30]
Basic model parameters	Model domain of 768 km, grid mash of 1.5 km, time step of 12 s and 33 vertical layers
Lateral boundary conditions	Cyclic
Initial conditions	The vertical profiles of initial temperature and specific humidity from the observations at 156 °E and 1.75 °S during TOGA COARE at 0400 LST 19 December 1992[31]
Model integration	0400 LST 22 December 1992–0400 LST 08 January 1993 (a selected period of TOGA COARE)
Large-scale forcing	Zero large-scale vertical velocity, vertically uniform zonal wind of 4 m·s^{-1}

Table 2. Sensitivity experiment designs. The control experiment (SST29) and four sensitivity experiments are imposed by time-invariant SST of 29 °C.

Experiment	Difference from SST29
SST29NWR	Water hydrometeor mixing ratios are set to zero in the calculation of radiation.
SST29NIR	Ice hydrometeor mixing ratios are set to zero in the calculation of radiation.
SST29NCR	Total hydrometeor mixing ratios are set to zero in the calculation of radiation.
SST29NIM	Ice hydrometeor mixing ratios are set to zero.

Table 3. Rain rates (mm·h^{-1}) averaged from day 31 to day 40 over model domain.

Experiment	SST29	SST29NWR	SST29NIR	SST29NCR	SST29NIM
Rain rate	0.130	0.146	0.186	0.198	0.124

Here, P_S is the surface rain rate; Q_{NC} is the net condensation, where $([P_{CND}]+[P_{DEP}]+[P_{SDEP}]+[P_{GDEP}])$ represents the cloud source term that consists of the vapor condensation rate for the growth of cloud water ($[P_{CND}]$), vapor deposition rates for the growth of cloud ice ($[P_{DEP}]$), snow ($[P_{SDEP}]$) and graupel ($[P_{GDEP}]$); $-([P_{REVP}]+[P_{MLTG}]+[P_{MLTS}])$ denotes the cloud sink term that includes the growth of vapor by evaporation of raindrop ($[P_{REVP}]$), evaporation of liquid from the graupel surface ($[P_{MLTG}]$) and evaporation of melting snow ($[P_{MLTS}]$); q_v is the specific humidity; u is the zonal wind; $q_5 = q_c + q_r + q_i + q_s + q_g$, q_c, q_r, q_i, q_s, q_g are the mixing ratios of cloud water, raindrops, cloud ice, snow and graupel, respectively; $[()](= \int_{z_b}^{z_t} \bar{\rho}()\,dz)$ is mass integration; z_t and z_b are the heights of the top and bottom of the model atmosphere respectively. Net condensation ($Q_{NC} > 0$) occurs when condensation and deposition rates are both higher than the evaporation rate of precipitation hydrometeors, whereas net evaporation ($Q_{NC} < 0$) appears when condensation and deposition rates are both lower than the evaporation rate of precipitation hydrometeors. Hydrometeor may have loss/convergence ($Q_{CM} > 0$) or gain/divergence ($Q_{CM} < 0$). Thus, surface rainfall can be separated into three types. Rainfall type CM has net condensation and hydrometeor loss/convergence, Cm has net condensation and hydrometeor gain/divergence and cM has net evaporation and hydrometeor loss/convergence.

3. Results

3.1. Control experiment

The contribution to the total rainfall from each rainfall type is denoted by the percentage of the rainfall amount of each rainfall type over the total rainfall amount (PRA). The calculation of PRA shows 14.2% for the rainfall (cM) associated with net evaporation and hydrometeor loss/convergence in SST29 (Fig. 1(a)), which is about half of PRA found in the COARE case with the large-scale forcing.[17] The COARE experiment was integrated from 0400 LST 22 December 1992 to 0400 LST 08 January 1993 during the westerly wind burst over an equatorial tropical area. The model used in the experiment was imposed by large-scale forcing derived from COARE observations. This implies that large-scale forcing enhances hydrometeor loss/convergence and associated rainfall. cM in SST29 has downward motions below 6 km and above 10 km whereas it has upward motions between 6 km and 10 km (Fig. 2(c)), which is different from upward motion above 6 km shown in the COARE case. The SST29 has the weaker downward water vapor and hydrometeor mass fluxes (Figs. 3(c) and 4(c)) in cM than the COARE case. The SST29 shows a positive specific-humidity perturbation in cM throughout the troposphere (Fig. 5(c)), whereas the COARE case reveals a weak negative specific-humidity perturbation near the surface. The positive specific-humidity perturbation associated with cM is at least one order of magnitude smaller in the SST29 case than in the COARE case. The SST29 and COARE cases have similar vertical profiles of a positive hydrometeor mixing ratio with a maximum around 6 km (Fig. 6(c)) but the former is about half of the latter.

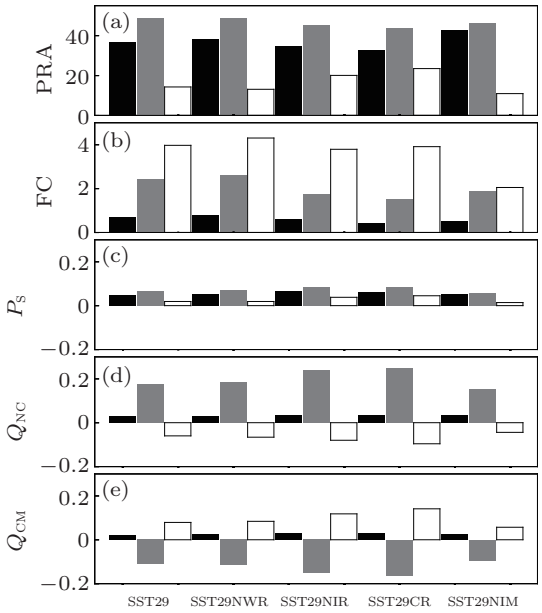


Fig. 1. (a) Percentage of rain amount over the total rainfall amount (PRA), (b) fractional coverage (FC) and model domain mean cloud budgets [(c) P_S, (d) Q_{NC}, (e) Q_{CM}] for CM (black bar), Cm (grey bar) and cM (open bar) in the SST29, SST29NWR, SST29NIR, SST29NCR, and SST29NIM cases. Units are % for FC and PRA and mm·h^{-1} for cloud budget.

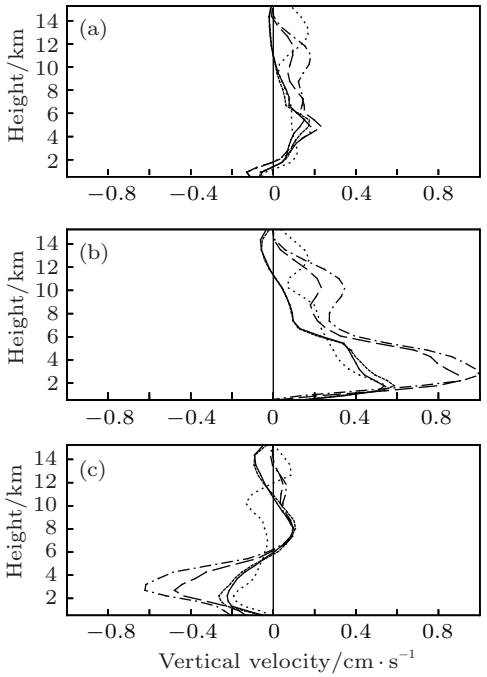


Fig. 2. Vertical profiles of time and model domain mean vertical velocity (cm·s^{-1}) in (a) CM, (b) Cm and (c) cM. Solid, short dash, long dash, dot dash and dot lines denote SST29, SST29NWR, SST29NIR, SST29NCR, and SST29NIM, respectively.

The rainfall (Cm) associated with net condensation and hydrometeor gain/divergence has larger PRA in the SST29 case than in the COARE case (Fig. 1(a)). Upward motions associated with Cm reach their maxima around 1 km in the SST29 case (Fig. 2(b)) and around 4.5 km in the COARE case. The SST29 case shows downward motions above 11 km, which is different from the upward motions in the COARE case. Cm has similar vertical profiles of upward water vapor mass flux with the maximum around 2 km in the SST29 and COARE case, although upward water vapor mass flux is smaller in the SST29 case than in the COARE case (Fig. 3(b)). The upward hydrometeor mass flux reaches its maximum around 2 km in the SST29 case (Fig. 4(b)), whereas it has its maximum around 3 km in the COARE case. The maximum is about three times smaller in the SST29 than in the COARE case. Cm has positive specific-humidity perturbations through the troposphere in the SST29 case (Fig. 5(b)), whereas it shows a large negative specific-humidity perturbation near the surface in the COARE case. Cm has maximum hydrometeor mixing ratios around 2 km and 6 km in the SST29 case (Fig. 6(b)), but it has a maximum hydrometeor mixing ratio around 5.5 km in the COARE case.

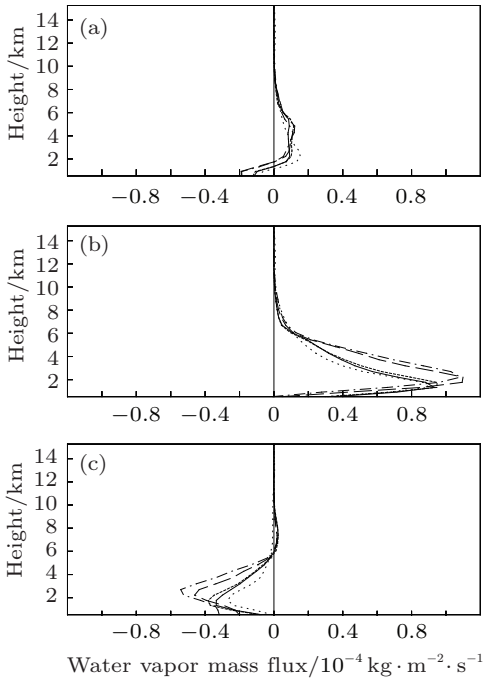


Fig. 3. The same as in Fig. 2 except for water vapor mass flux (10^{-4} kg·m^{-2}·s^{-1}).

The rainfall (CM) associated with net condensation and hydrometeor loss/convergence has similar PRAs in the SST29 and COARE cases. Both cases also show similar vertical profiles of vertical velocity and associated water vapor and hydrometeor mass fluxes (Figs. 2(a)–4(a)). The SST29 case has positive specific-humidity perturbations throughout the troposphere (Fig. 5(a)), but the COARE case has a negative specific-humidity perturbation near the surface. Both cases show similar vertical profiles of the hydrometeor mixing ratio (Fig. 6(a)).

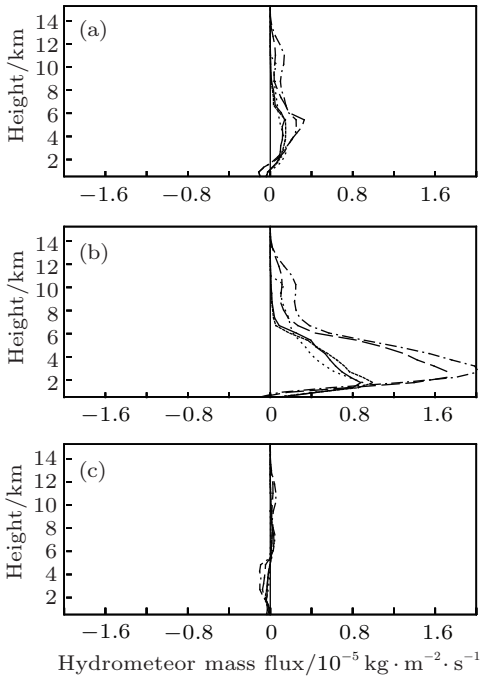


Fig. 4. The same as in Fig. 2 except for hydrometeor mass flux (10^{-5} kg·m^{-2}·s^{-1}).

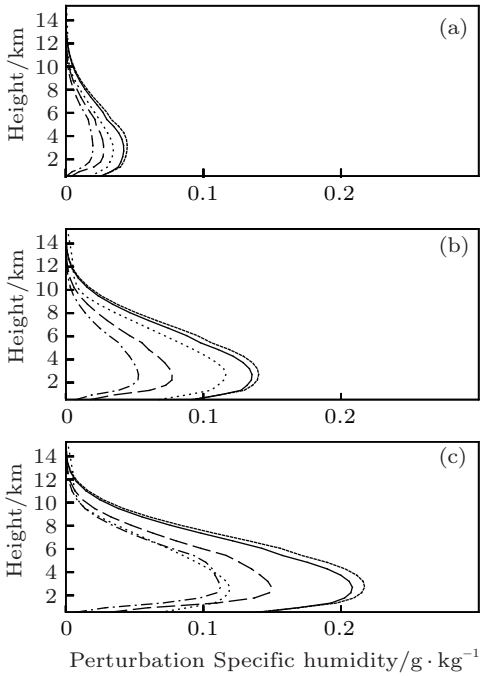


Fig. 5. The same as in Fig. 2 except for perturbation specific humidity (g·kg^{-1}).

The PRA in the SST29 case is larger in Cm than in CM because Cm occupies a larger rainfall area than CM (Fig. 1(b)). Although cM covers a larger rainfall area than the other rainfall types, its rain rate is lower than those of CM and Cm (Fig. 1(c)). The small rain rate of cM is caused by a large offset between net evaporation and hydrometeor loss/convergence

(Figs. 1(d) and 1(e)). The breakdown of CM into CM1 and CM2 reveals that although CM1 and CM2 cover equal rainfall areas, CM1 has a larger PRA than CM2 in the SST29 case (Fig. 7), which is different from equal PRAs of CM1 and CM2 in the COARE case. The rain rate of CM1 is 50% higher than that of CM2 because the net condensation rate is about three times higher in CM1 than in CM2, but hydrometeor loss/convergence rate in CM1 is about half of that in CM2.

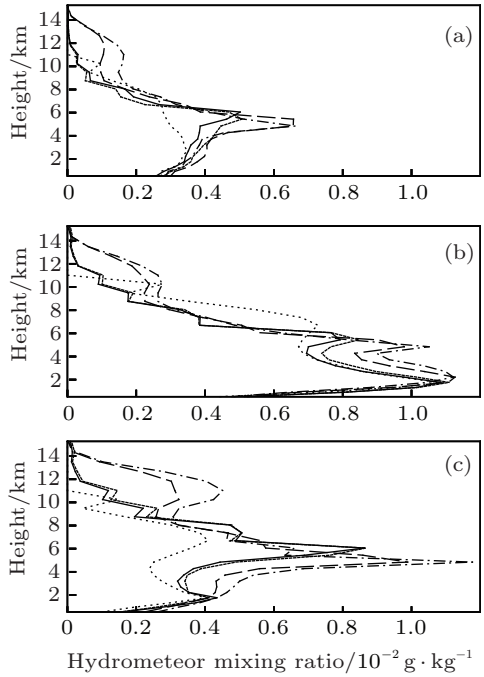


Fig. 6. The same as in Fig. 2 except for hydrometeor mixing ratio (10^{-2} g·kg^{-1}).

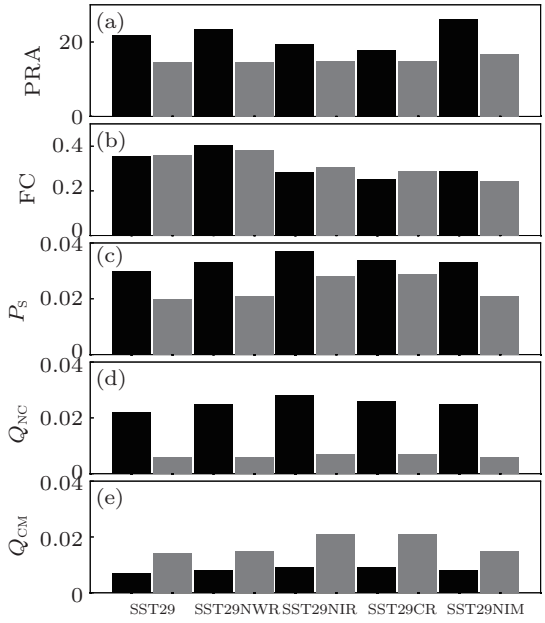


Fig. 7. Breakdown of CM into CM1 (black bar) and CM2 (grey bar) for (a) percentage of rain amount over total rainfall amount (PRA), (b) fractional coverage (FC) and model domain mean cloud budgets [(c) P_S, (f) Q_{NC}, (e) Q_{CM}] in the SST29, SST29NWR, SST29NIR, SST29NCR, and SST29NIM cases. Units are % for FC and PRA and mm·h^{-1} for cloud budget.

3.2. Effects of ice clouds

The comparison between SST29 and SST29NIM shows that the exclusion of ice clouds increases the PRA of CM whereas it reduces the PRAs of Cm and cM (Fig. 1). The increase in the rainfall contribution of CM is associated with the increase in rain rate caused by the increase in net condensation although the removal of ice clouds reduces rainfall area of CM. The increase in rainfall contribution of CM comes from both CM1 and CM2 due to the increases in their rain rates caused by the increase in net condensation in CM1 and the enhancement in hydrometeor loss/convergence in CM2 (Fig. 7). The decreases in rainfall contributions of Cm and cM are related to the shrinking of rainfall areas. The exclusion of ice clouds significantly reduces the net condensation of Cm and hydrometeor loss/convergence of cM (Fig. 1).

The upward motions of CM above 10 km increase from SST29 to SST29NIM while they are suppressed in the mid troposphere (Fig. 2). The vertical velocities of Cm and cM above 11 km switch from downward motions in the SST29 case to upward motions in the SST29NIM case. The upward motions of Cm between 6 km and 11 km increase from the SST29 case to the SST29NIM case, whereas those below 6 km decrease. The vertical velocity of cM between 6 km and 10 km switches from upward motions in the SST29 case to downward motions in the SST29NIM case. The downward motions of cM below 6 km are slightly weaker in the SST29NIM than in the SST29 case. The exclusion of ice clouds increases upward water vapor mass flux of CM below 4 km whereas it reduces upward water vapor mass flux of CM above 4 km (Fig. 3). The removal of ice clouds reduces upward water vapor mass flux of Cm and downward water vapor mass flux of cM. Weak hydrometeor mass fluxes of CM and cM are similar in the case SST29 to those in the SST29NIM case (Fig. 4). The exclusion of ice clouds suppresses upward hydrometeor mass flux of Cm below 6 km whereas it enhances upward hydrometeor mass flux of Cm above 6 km. The elimination of ice clouds reduces positive specific humidity perturbation from the SST29 case to the SST29NIM case (Fig. 5). Without considering the action of ice clouds, the positive hydrometeor mixing ratio between Cm and cM above 6 km is decreasing, and so is the hydrometeor mixing ratio of CM throughout the troposphere. Without considering the action of ice clouds, the positive hydrometeor mixing ratio between Cm and cM above 6 km is decreasing, and so is the hydrometeor mixing ratio of CM throughout the troposphere.

The effects of ice clouds include radiative and microphysical effects of ice clouds. Exclusion of the radiative effects of ice clouds significantly increases the rainfall contribution of cM from the SST29 case to the SST29NIR case through the increase in rain rate, whereas it reduces rainfall contributions of CM and Cm through the shrinking of rainfall areas (Fig. 1). The reduction in rainfall contribution of CM comes

from the increase in rainfall contribution of CM1 due to the shrinking of rainfall area (Fig. 7). Exclusion of the radiative effects of ice clouds increases net condensation of CM and Cm through the increase in the mean infrared radiative cooling[16] and enhances associated hydrometeor loss/convergence of cM (Fig. 1). Exclusion of the radiative effects of ice clouds increases the upward motions and water vapor mass flux of CM above 2 km, upward motions and water vapor mass flux of Cm throughout the troposphere, and downward motions and water vapor mass flux of cM below 6 km (Figs. 2 and 3). Removal of the radiative effects of ice clouds enhances downward motions and water vapor mass flux of CM near the surface. Upward hydrometeor mass fluxes of CM and Cm are larger in the SST29NIR case than in the SST29 case (Fig. 4). Downward hydrometeor mass fluxes of cM are small in both SST and SST29NIR. The positive specific humidity perturbations are smaller in the SST29NIR case than in the SST29 case for all rainfall types (Fig. 5), implying more consumption of water vapor in the production of rainfall in the SST29NIR case than in the SST29 case. This can be demonstrated by the general increases in hydrometeor mixing ratios from the SST29 case to the SST29NIR case for all rainfall types (Fig. 6).

The exclusion of microphysical effects of ice clouds reduces the rainfall contribution of cM from the SST29NIR case to the SST29NIM case, whereas it increases the rainfall contribution of CM (Fig. 1). The rainfall contribution of Cm is less sensitive to microphysical effects of ice clouds than those of the two other rainfall types. The reduction in rainfall contribution of cM is associated with the reduction in both rainfall and its area when hydrometeor loss/convergence is significantly reduced by the exclusion of microphysical effects of ice clouds. The increase in rainfall contribution of CM results primarily from the increase in rainfall contribution of CM1 through the expansion of the rainfall area (Fig. 7). Removal of the microphysical effects of ice clouds significantly reduces net condensation of cM and associated hydrometeor loss/convergence of cM (Fig. 1).

In CM, removal of the microphysical effects of ice clouds reduces downward motions near the surface and upward motions between 4 km and 11 km, whereas it increases upward motions between 1 km and 4 km and above 11 km (Fig. 2). In Cm, removal of the microphysical effects of ice clouds suppresses upward motions below 12 km, whereas it enhances upward motions above 12 km. In cM, elimination of the microphysical effects of ice clouds reduces downward motions below 6 km, switches upward motions in SST29NIR to downward motions in the SST29NIM case and increases upward motions above 12 km. Removal of the microphysical effects of ice clouds weakens upward water vapor mass flux of Cm and downward water vapor mass flux in cM, whereas it reduces downward water vapor mass flux near the surface and increases upward water vapor mass flux between 1 km and 4 km (Fig. 3). Elimination of the microphysical effects of ice clouds reduces upward hydrometeor mass fluxes of Cm and CM, and weakens downward hydrometeor mass flux of cM (Fig. 4). Exclusion of the microphysical effects of ice clouds enhances positive specific humidity perturbation of CM and Cm, whereas it reduces positive specific humidity perturbation of cM (Fig. 5). Exclusion of the microphysical effects of ice clouds generally reduces hydrometeor mixing ratios for all rainfall types except that it enhances the hydrometeor mixing ratio of Cm at 6 km to that at 9 km (Fig. 6).

3.3. Effects of water clouds

Exclusion of the radiative effects of water clouds increases the rainfall contribution of CM from the SST29 case to the SST29NWR case through the expansion of the rainfall area in the presence of the radiative effects of ice clouds, whereas it reduces the rainfall contribution of CM from the SST29NIR case to the SST29NCR case through the shrinking of the rainfall area in the absence of the radiative effects of ice clouds (Fig. 1). The increase in the rainfall contribution of CM from the SST29 case to the SST29NWR case and the reduction in the rainfall contribution of CM from the SST29NIR case to the SST29NCR case result, respectively, from the increase and reduction in the rainfall contribution of CM1 (Fig. 7) caused by the expansion and shrinking of the rainfall area. Removal of the radiative effects of water clouds reduces the rainfall contribution of Cm through the reduction in the rain rate in the presence of the radiative effects of ice clouds and the shrinking of the rainfall area in the absence of the radiative effects of ice clouds. The rainfall reduction of Cm is associated with the increase in hydrometeor gain/divergence from the SST29 case to the SST29NWR case. Removal of the radiative effects of water clouds increases the net condensation of CM and Cm through the increase in infrared radiative cooling[16] and associated hydrometeor loss/convergence of cM in the presence of the radiative effects of ice clouds (Fig. 1). Elimination of the radiative effects of water clouds reduces the rainfall contribution of cM through the reduction in the rain rate in the presence of the radiative effects of ice clouds, but it increases the rainfall contribution of cM through the increases in rainfall and its area in the absence of the radiative effects of ice clouds. Exclusion of the radiative effects of ice clouds increases the net condensation of Cm and associated with hydrometeor loss/convergence of cM in the absence of the radiative effects of ice clouds (Fig. 1).

Exclusion of the radiative effects of water clouds strengthens upward motions of CM and Cm between 1 km and 6 km in the presence of the radiative effects of ice clouds and throughout the troposphere in the absence of the radiative effects of ice clouds (Fig. 2). Removal of the radiative effects of water clouds intensifies downward motions of cM between 1 km and 6 km regardless of the radiative effects of

ice clouds. The vertical velocity is more sensitive to the radiative effects of water clouds in the absence of the radiative effects of ice clouds than in the presence of the radiative effects of ice clouds. Exclusion of the radiative effects of water clouds increases upward water vapor and hydrometeor mass fluxes of CM and Cm and downward water vapor and hydrometeor mass fluxes of cM (Figs. 3 and 4). Elimination of the radiative effects of water clouds slightly increases positive specific humidity perturbations in the presence of the radiative effects of ice clouds, but it significantly reduces positive specific humidity perturbations in the absence of the radiative effects of ice clouds (Fig. 5). Removal of the radiative effects of water clouds increases more hydrometeor mixing ratios for all rainfall types in the absence of the radiative effects of ice clouds than in the presence of the radiative effects of ice clouds (Fig. 6).

4. Comparison discussion

The rainfall can be partitioned into convective and stratiform components using the scheme originally developed by Tao *et al.*[6] and modified by Sui *et al.*[7] In the control experiment, while convective and stratiform rainfalls are equal contributors to CM, Cm and cM primarily convective and stratiform rainfalls, respectively (Table 4). Exclusion of the radiative effects of ice clouds increases the contributions of convective rainfall to all three rainfall types, whereas the removal of the microphysical effects of ice clouds increases the contribution of convective rainfall to CM and the contribution of stratiform rainfall to Cm. All three rainfall types show large contributions from convective rainfall because exclusion of the microphysical effects of ice clouds severely weakens the development of stratiform clouds and associated rainfall. Exclusion of the radiative effects of water clouds enhances the contribution of convective rainfall to all three rainfall types, regardless of the radiative effects of ice clouds.

Shen *et al.*[10] partitioned rainfall into eight types based on surface rainfall budget (see Table 5). In the control experiment, CM and Cm are primarily attributable to TFM and TFm, respectively (Fig. 8), which are different from those found in Li *et al.*[17] cM is primarily associated with TfM, which is similar to that found in Li *et al.*[17] Exclusion of the radiative effects of ice clouds reduces the contributions of TFM and TFm to CM and Cm, respectively, whereas it increases the contribution of TfM to cM. Removal of the microphysical effects of ice clouds increases the contributions of TFM and TfM to CM and cM, respectively, whereas it reduces the contribution of TFm to Cm. In the presence of the radiative effects of ice clouds, exclusion of the radiative effects of water clouds increases the contributions of TFM and TfM to CM and cM, respectively, whereas it does not affect the contribution of TFm to Cm. In the absence of the radiative effects of ice clouds, removal of the radiative effect of water clouds reduces the contribution of TFM to CM, whereas it increases the contributions of TFm and TfM to Cm and cM, respectively.

Table 4. Percentage (%) of (a) convective and (b) stratiform rainfall over rainfall amount from CM, Cm, and cM in the SST29, SST29NWR, SST29NIR, SST29NCR, and SST29NIM cases.

(a)	SST29	SST29NWR	SST29NIR	SST29NCR	SST29NIM
CM	53.7	60.5	70.3	76.3	75.0
Cm	75.7	77.1	86.7	88.1	77.1
cM	36.1	39.3	40.5	44.2	63.2
(b)	SST29	SST29NWR	SST29NIR	SST29NCR	SST29NIM
CM	46.3	39.5	29.7	23.7	25.0
Cm	24.3	22.9	13.3	11.9	22.9
cM	63.9	60.7	59.5	55.8	36.8

Table 5. Summary of rainfall types partitioned based on surface rainfall budget. T and t represent local atmospheric drying and moistening, respectively. F and f denote water vapor convergence and divergence, respectively. M and m refer to hydrometeor loss/convergence and gain/divergence, respectively.

Type	Description
TFM	Water vapor convergence, local atmospheric drying, and hydrometeor loss/convergence
TFm	Water vapor convergence, local atmospheric drying, and hydrometeor gain/divergence
tFM	Water vapor convergence, local atmospheric moistening, and hydrometeor loss/convergence
tFm	Water vapor convergence, local atmospheric moistening, and hydrometeor gain/divergence
TfM	Water vapor divergence, local atmospheric drying, and hydrometeor loss/convergence
Tfm	Water vapor divergence, local atmospheric drying, and hydrometeor gain/divergence
tfM	Water vapor divergence, local atmospheric moistening, and hydrometeor loss/convergence
tfm	Water vapor divergence, local atmospheric moistening, and hydrometeor gain/divergence

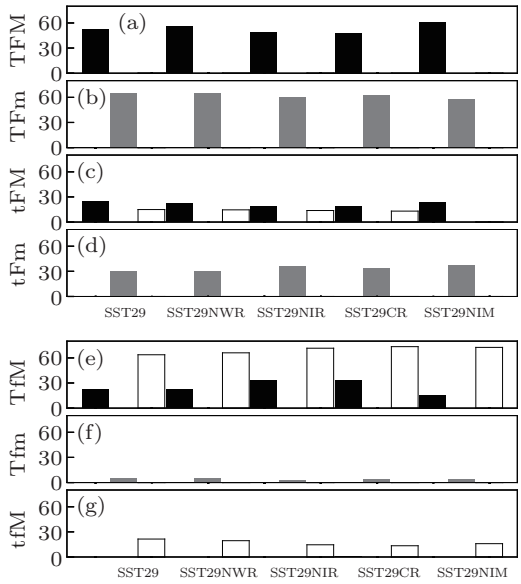


Fig. 8. Percentage (%) of seven rainfall types [(a) TFM, (b) TFm, (c) tFM, (d) tFm, (e) TfM, (f) Tfm and (g) tfM] partitioned based on the surface rainfall budget (Shen *et al.* 2010b) over the rainfall amount from CM (black bar), Cm (grey bar), nd cM (open bar) in the SST29, SST29NWR, SST29NIR, SST29NCR, and SST29NIM cases.

5. Summary

The effects of water and ice clouds on the cloud microphysical budget of equilibrium precipitation are investigated through an analysis of the grid-scale equilibrium simulation data from a series of sensitivity experiments imposed without large-scale vertical velocity. The major results are shown as follows.

(I) In the control experiment, the rainfall (Cm) with net condensation and hydrometeor gain/divergence makes the largest contribution to the total rainfall in the three rainfall types. The contribution from rainfall (cM) with net evaporation and hydrometeor loss/convergence is about one third of that from Cm and about half that from the rainfall (CM) with net condensation and hydrometeor loss/convergence.

(II) Exclusion of ice clouds reduces the rainfall contribution from cM and Cm, respectively, but elimination of the microphysical and radiative effects of ice clouds increases the rainfall contribution from CM through the removal of the microphysical effects of ice clouds. The reduction in the rainfall contribution of cM caused by the removal of the microphysical effects of ice clouds is associated with the reduction in rainfall and its area. The reduced rainfall contribution of Cm resulting from the exclusion of the radiative effects of ice clouds is related to the shrinking of the rainfall area.

(III) Radiative effects of water clouds on rainfall contribution of each rainfall type depend on the radiative effects of ice clouds. In the presence of the radiative effects of ice clouds, the exclusion of radiative effects of water clouds increases the rainfall contribution of CM through the expansion of the rainfall area but it reduces the rainfall contribution of cM through the reduction in rainfall and its area. The rainfall contribution of Cm is insensitive to the radiative effects of water clouds. In the absence of the radiative effects of ice clouds, removal of the radiative effects of water clouds enhances the rainfall contribution of cM through the increase in rainfall and its area, whereas it reduces the rainfall contributions of CM and Cm through the shrinking of rainfall areas.

Acknowledgment

The authors thank Dr. W. K Tao at NASA/GSFC for his cloud resolving model.

References

[1] Li X, Sui C H and Lau K M 2002 *Mon. Wea. Rev.* **130** 2481
[2] Houghton H G 1968 *J. Appl. Meteor.* **7** 851
[3] Churchill D D and Houze R A 1984 *J. Atmos. Sci.* **41** 933
[4] Caniaux G, Redelsperger J L and Lafore J P 1994 *J. Atmos. Sci.* **51** 2046
[5] Steiner M, Houze R A and Yuter S E 1995 *J. Appl. Meteor.* **34** 1978
[6] Tao W K, Simpson J, Sui C H, Ferrier B, Lang S, Scala J, Chou M D and Pickering K 1993 *J. Atmos. Sci.* **50** 673
[7] Sui C H, Lau K M, Tao W K and Simpson J 1994 *J. Atmos. Sci.* **51** 711
[8] Cui X and Li X 2006 *J. Geophys. Res.* **111** D17112
[9] Gao S, Cui X, Zhou Y and Li X 2005 *J. Geophys. Res.* **110** D10202
[10] Shen X, Wang Y, Zhang N and Li X 2010 *J. Geophys. Res.* **115** D24205
[11] Li X and Gao S 2011 *Precipitation Modeling and Quantitative Analysis* (Berlin: Springer Press)
[12] Gao S, Zhou Y and Li X 2007 *J. Atmos. Sci.* **64** 656
[13] Ping F, Luo Z and Li X 2007 *Mon. Wea. Rev.* **135** 2794
[14] Gao S 2008 *J. Geophys. Res.* **113** D03108, doi: 10.1029/2007JD009177
[15] Gao S and Li X 2008 *Cloud-resolving Modeling of Convective Processes* (Berlin: Springer Press)
[16] Zhou Y and Li X 2011 *Adv. Atmos. Sci.* **28** 1099
[17] Li X, Shen X and Liu J 2011 *Atmos. Res.* **102** 444
[18] Soong S T and Ogura Y 1980 *J. Atmos. Sci.* **37** 2035
[19] Soong S T and Tao W K 1980 *J. Atmos. Sci.* **37** 2016
[20] Tao W K and Simpson J 1993 *Terr. Atmos. Oceanic Sci.* **4** 35
[21] Li X, Sui C H, Lau K M and Chou M D 1999 *J. Atmos. Sci.* **56** 3028
[22] Sui C H, Li X and Lau K M 1998 *J. Atmos. Sci.* **55** 2345
[23] Lin Y L, Farley R D and Orville H D 1983 *J. Climate Appl. Meteor.* **22** 1065
[24] Rutledge S A and Hobbs P V 1983 *J. Atmos. Sci.* **40** 1185
[25] Rutledge S A and Hobbs P V 1984 *J. Atmos. Sci.* **41** 2949
[26] Tao W K, Simpson J and McCumber M 1989 *Mon. Wea. Rev.* **117** 231
[27] Krueger S K, Fu Q, Liou K N and Chin H N S 1995 *J. Appl. Meteor.* **34** 281
[28] Chou M D, Suarez M J, Ho C H, Yan M M H and Lee K T 1998 *J. Atmos. Sci.* **55** 201
[29] Chou M D, Kratz D P and Ridgway W 1991 *J. Climate* **4** 424
[30] Chou M D and Suarez M J 1994 *NASA Tech. Memo.* **3** 85
[31] Sui C H, Lau K M, Takayabu Y N and D Short 1997 *J. Atmos. Sci.* **54** 639